

# Monte Carlo analytical-geometrical simulation of piezoresistivity and electrical conductivity of polymeric nanocomposites filled with hybrid carbon nanotubes/graphene nanoplatelets



M. Haghgoor<sup>a</sup>, R. Ansari<sup>a,\*</sup>, M.K. Hassanzadeh-Aghdam<sup>b,\*</sup>

<sup>a</sup> Faculty of Mechanical Engineering, University of Guilan, Rasht, Iran

<sup>b</sup> Department of Engineering Science, Faculty of Technology and Engineering, East of Guilan, University of Guilan, Rudsar-Vajargah, Iran

## ARTICLE INFO

### Keywords:

- A. Multifunctional composites
- B. Nanocomposites
- C. Electrical properties
- D. Analytical modeling

## ABSTRACT

Piezoresistivity and electrical conductivity of carbon nanotube (CNT)/graphene nanoplatelet (GNP)-filled polymer nanocomposites are investigated using a 3D Monte Carlo analytical-geometrical model. GNPs and CNTs are considered as randomly distributed solid thin rectangular cube and cylinder, respectively. After establishment of a random CNT/GNP network, electrical conductivity and relative resistance change with strain is calculated. Model considers effect of CNT and GNP deformation on filler separation distance as the dominant factor for percolation tunneling. Comparing model results with experimental data of hybrid nanocomposites showed a good agreement for electrical conductivity and piezoresistivity. Analytical model is developed on the basis of geometrical tunneling percolation theory to consider the effect of several parameters like height of barrier potential, GNP side length, CNT orientation and dimensions on electric behavior of nanocomposites. Results revealed that CNT dispersion state and GNP dimensions have significant effects on the percolation threshold and resistivity change ratio of nanocomposites with strain.

## 1. Introduction

A new class of conductive nanocomposite made by incorporation of electrically conductive fillers in a polymer matrix is used in electrochromic devices, strain-detecting sensors, supercapacitors, and electromagnetic interference shielding [1,2]. Combining conductive fillers (e.g. CNT and GNP) could improve filler network conductivity because the conductivity of filler is much higher than that of a matrix [3,4]. CNTs provide high-strength and large surface area with special 1D physical structure ideal for conductivity and GNPs offer excellent conductivity with 2D high aspect ratio structure ideal for gathering many types of contact for charge transport capability [5,6]. Hybrid nanocomposite with two or more fillers of different geometric shapes, dimensions and aspect ratios could achieve better conductivity and lower cost than those reinforced with either CNTs or GNPs alone (unary composites) [2]. Fillers with different geometries can affect the 3D network structure formation and bring various capabilities such as great strength and conductivity to nanocomposite [7,8]. Bridging of CNT network between GNPs could improve the network percolation by quantum tunneling which plays a dominant role in the electrical transport of CNT based

nanocomposite through a percolation process [9,10]. At low volume fractions, the nano-fillers are too far apart and the electrical conductivity is low. The low electrical conductivity is due to the small number of fillers linked together. Therefore, the fillers are not electrically related to each other. The isolated fillers decrease distance with the increase of the number of adjacent fillers [11]. In this situation, tunneling happens between neighboring fillers leading to gradual increase in the conductivity of nanocomposite. After that a complete electrical path is formed due to the enlarged number of fillers, the electrical conductivity of composite enhances abruptly which this rapid increment in electrical conductivity is known as percolation behavior [12]. Electrical conductivity in CNT reinforced nanocomposite is widely specified by this percolation event, which originates from the distributions of both insulating and conducting phases with hugely different electrical properties [13,14].

Addition of a small amount of CNT/GNP fillers to polymer improves the piezoresistivity by keeping interfacial bonds during strain while maintaining the light weight of composite [15]. Piezoresistive materials are able to translate stress into a convertible signal [16]. Nanocomposites whose piezoresistive behavior has been increased with CNT/

\* Corresponding authors.

E-mail addresses: [r\\_ansari@guilan.ac.ir](mailto:r_ansari@guilan.ac.ir) (R. Ansari), [mk.hassanzadeh@gmail.com](mailto:mk.hassanzadeh@gmail.com) (M.K. Hassanzadeh-Aghdam).

GNP incorporation are promising for applications such as strain sensing, health and fitness monitoring [17–19]. These high aspect ratio nano-fillers (CNT and GNP) are the most suitable conductors for highly flexible strain sensing applications [20]. The GNPs have very efficient reinforcing capability due to their 2D parallel alignment in the stretching plane, while CNT has the most robust conductive network formation during stretching due to more interactions of the 1D structures [21]. Thus, the hybrid fillers can form a structure in which the GNPs with great entanglement capability bundle CNTs in the formation of conductive network [22,23]. These local bonding are promising for piezoresistivity due to the high surface area along 2D geometry of GNP and long distance charge transmission capability of 1D CNTs [24,25]. The strain sensitive conductivity is emanated from the destruction of the CNT/GNP conductive paths. Therefore, piezoresistivity happens due to the synergistic interaction between GNP and CNT which increases load bearing capability and compensates poor strength of polymer to loads [14,21].

Analytical models including percolation theory has preference over time consuming numerical methods. Many analytical models predict electrical conductivity based on the shape of nanofillers, orientation of CNT and tunneling resistance between them. Recently, various analytical models are presented to study the electrical conductivity and piezoresistivity of polymer based carbon nanocomposites.

Rahman and Servati [26] developed a model for CNT-polymer conductivity considering the effect of inter-tube tunneling through the polymer. They investigated the statistical effects of inter-tube distance and alignment on the tunneling. They presented a numerical model for the tunneling resistance as a function of CNT concentration and polymer properties. They reported that piezoresistivity increases non-linearly with increasing strain and this enhancement diminishes with lower orientation angle. Wang and Ye [27] numerically investigated the mechanism and optimization of piezoresistive CNT-polymer composites. They introduced average junction gap as a quantitative description of the conductance variation of a CNT network to study the parameters of CNT and polymer on piezoresistivity. Their numerical results showed that the junction resistances between CNTs are a major component of the network conductance of the composite. Feng et al. [28] studied the bi-axial stretching effects on the electrical conductivity of CNT composites by a mixed micromechanics model with the consideration of the electrical conductive mechanisms. They considered the bi-axial stretching effects by volume expansion of composite, re-orientation of CNTs and change of conductive networks. They reported that bi-axial stretching decreased the electrical conductivity of composite due to dominant role of the stretching induced change in conductive networks. They found that the decreasing rate of electrical conductivity enhanced in the bi-axial stretching plane. Souri et al. [29] carried out a theoretical study of polymeric nanocomposite based on the self-consistent effective medium theory to provide physical insight into complex material systems. They adopted the effects of the interface and tunneling effects to demonstrate that the overall piezoresistive sensitivity reduces when the lower interfacial resistivity of CNTs is considered. They investigated the effects of MWCNT weight percentage, length and tunneling effects on the piezoresistivity of the nanocomposite. Xiang et al. [30] fabricated a high-performance strain sensor of CNT polymer nanocomposite. They established a conductive model to study the electro-mechanical properties of the strain sensor based on Simmons' tunneling theory. They reported that the sensor sensitivity was greatly improved with the addition of low content uniformly dispersed CNTs. Fang et al. [31] investigated an analytical model to describe the influence of mechanical deformation on the effective electrical conductivity of CNT reinforced composites. Strain-induced change of the electrical conductivity illustrated the effect of mechanical strain on the effective electrical conductivity. They treated both the strain-induced volume fraction change of inclusions and the strain-induced tunneling conductivity change of CNTs as the linear functions of the strain. They reported that the effect of the strain on the electrical conductivity diminishes with higher volume

fraction of CNTs. Tang et al. [32] predicted the electro-mechanical response of conductive CNT-based composite by considering CNT dimensions, interphase and dispersion state. They considered the stretching-induced changes in the model by the variation of CNT content, CNT orientation, and percolated conductive network. They considered the key factors including filler geometry, interphase region, filler dispersion, Poisson's ratio and barrier height in affecting the piezoresistive response of CNT-based composite sensors. They declared that the piezoresistive sensitivity of the nanocomposite increased with filler content above the percolation threshold and higher matrix barrier height.

The above-mentioned literature review demonstrates that there have been many analytical studies on the piezoresistive response of single filler nanofiller modified composites. However, very limited analytical work exists in literature to explain the piezoresistive response of hybrid nanocomposite. This work presents a Monte Carlo analytical-geometrical percolation network model to study the effect of strain on the resistivity change of hybrid CNT/GNP polymer nanocomposite. In this analytical model, the straight and uniformly dispersed CNTs interact with thin rectangular GNPs. The coupling between the electrical and structural response representing the macro-scale nanocomposite is obtained by firstly evaluating the new positions of fillers and secondly calculating the electrical resistivity between them. The predicted results are compared with previous experimental data. Results show that the current analytical model agrees well with the experimental data reflecting the capability of the model to predict the piezoresistivity of conductive network composed of many conductive paths each formed by separated conductive fillers with lots of contacts between them. At the end, the parametric studies are represented to show the changes of electrical conductivity and piezoresistive sensitivity of hybrid polymer nanocomposite providing links between nano-scale network features such as the aspect ratio, alignment, distribution and geometries of CNTs and GNPs and macro-scale electro-mechanical response.

## 2. Model generation

### 2.1. Integration of CNTs

In this section, an analytical model is prepared based on the inter-particle distance variation to predict the resistance change ratio occurred in CNT/GNP polymer nanocomposite due to a mechanical strain. Evaluation of changes in mutual position and contacts of fillers is the easiest way to establish a relationship between electrical properties of a material and its deformational state. For this, consideration of various parameters concerned with the geometrical connection configuration is needed. At first, the CNT distribution state that coincides with the geometrical contact configuration of CNTs spread in the insulating polymer is attained. For this, an RVE of the CNT dispersed in the matrix is presented.

**Fig. 1** shows 3D cubic RVE with CNTs and GNPs. The dimensions of the RVE are  $L_x \times L_y \times L_z (10 \times 10 \times 10 \mu\text{m}^3)$ , large enough to contain many fillers but small compared to the length over which the deformation could vary [33]. RVE consist of polymer matrix, CNT and GNP in which cylindrical CNT with length of  $l$  and a diameter of  $d$  and GNPs with side length of  $S$  and thickness of  $t$  are distributed in the polymer matrix. The number of fillers in the 3D RVE is set by their assigned volume fraction ( $10^{-15} \cdot V_f / \pi r^2 l$ ). For a newly generated CNT, if the ending point is located outside of the RVE, it is removed and will be substituted with a new one which fulfills the RVE limited space condition. In this study for the sake of simplifying the calculation, the distortion of CNT and wrinkle of GNP are ignored, and also the hard-core models for CNT and GNP lead to non-penetrating fillers.

Based on the 3D Monte Carlo model, a random distribution of CNTs is generated in the 3D RVE. Conductive 1D CNT can transport electrons by tunneling and contact. This conductive CNT is free from defect and

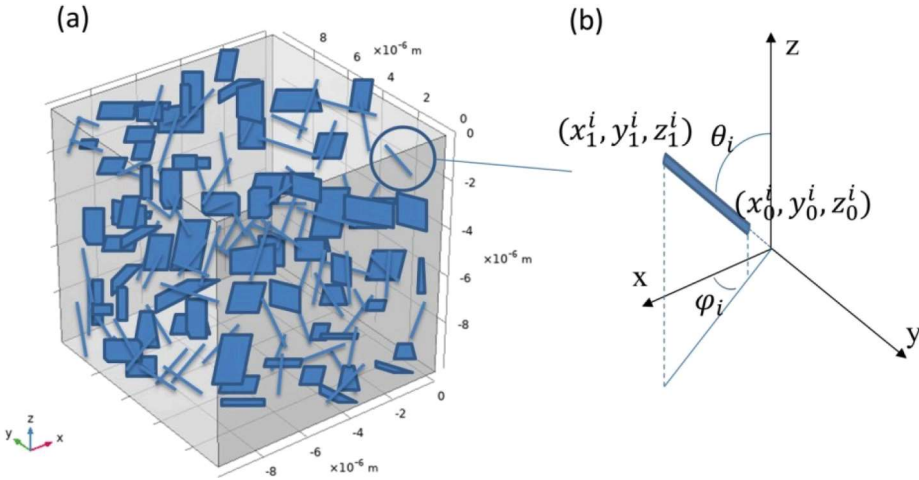


**Fig. 1.** Schematic of (a) a CNT/GNP hybrid nanocomposite (b) the  $i$  th randomly oriented CNT.

structurally perfect and the surrounding polymer is not affecting its electrical properties. CNT dispersion state has an important effect on its electrical properties. Every CNT added in the model can be described by a line segment with a starting point  $(x_0^i, y_0^i, z_0^i)$  and an ending point  $(x_1^i, y_1^i, z_1^i)$  such that.

$$\begin{Bmatrix} x_0^i \\ y_0^i \\ z_0^i \end{Bmatrix} = \begin{Bmatrix} x_0^i \\ y_0^i \\ z_0^i \end{Bmatrix} + \begin{Bmatrix} l_i \sin \theta_i \cos \varphi_i \\ l_i \sin \theta_i \sin \varphi_i \\ l_i \cos \theta_i \end{Bmatrix} \quad (1)$$

where  $l_i$ ,  $\varphi_i$  and  $\theta_i$  are the length, azimuthal and polar angles of the  $i$  th CNT, respectively. Here  $x_1^i$ ,  $y_1^i$ ,  $z_1^i$ ,  $\varphi^i$  and  $\theta_i$  follow a uniform distribution as drafted in Eq. (2).

$$\begin{Bmatrix} x_0^i \\ y_0^i \\ z_0^i \\ \varphi_i \\ \theta_i \end{Bmatrix} = \begin{Bmatrix} L \times \text{rand} \\ L \times \text{rand} \\ L \times \text{rand} \\ 2\pi \times \text{rand} \\ \cos^{-1}(2 \times \text{rand} - 1) \end{Bmatrix} \quad (2)$$

Here "rand" denotes some random number in the interval  $(0,1)$  and  $L$  is the side length of RVE.

The network resistance includes both intrinsic resistance of CNT and tunneling resistance between CNTs. The intrinsic resistance of a CNT is  $R_f = \frac{4l}{\sigma_f \pi d^2}$ . Where  $d$  is CNT diameter and  $\sigma_f$  is the CNT intrinsic electrical conductivity determined experimentally.

The contact region between two CNTs is at the nanoscale, the dimension of which can be less than the Fermi wavelength  $\lambda_F \approx 0.74 \text{ nm}$ . As such, the electron tunneling through the contact junction is in ballistic transport range, the current-voltage characteristic is given by the Landauer-Büttiker formula [34] as depicted in Eq. (3).

$$I = \frac{2e}{h} \int \tau M [f(E - eV) - f(E)] dE \quad (3)$$

Using  $f = \left\{ 1 + \exp\left(\frac{E - E_F}{k_B T}\right) \right\}^{-1}$  known as Fermi-Dirac distribution function, where  $E_F$  is the Fermi energy, Eq. (3) can be written as drafted in Eq. (4) [35].

$$I = \frac{2e}{h} \int_0^\infty \tau M \left[ \frac{1}{e^{\frac{E-\mu-eV}{k_B T}} + 1} - \frac{1}{e^{\frac{E-\mu}{k_B T}} + 1} \right] dE \quad (4)$$

Here,  $M$  is the total number of conduction channels and the symbol  $\tau$  denotes a transmission probability for the electron to tunnel through the polymer obstacle between a CNT and a GNP. Both of them are functions of electron energy level  $E$ . The quantities  $T$  and  $\mu$  represent the respective temperature and the chemical potential of the CNT. Other constants are the electron charge  $e (1.6022 \times 10^{-19} \text{ C})$ , Planck's constant  $h (6.6261 \times 10^{-34} \text{ Js})$ , and Boltzmann constant  $k_B$ . The symbol  $\tau$  is the electron transmission probability which can be estimated by solving the Schrödinger equation with rectangular potential barrier. If the minimum distance between walls of a pair of CNTs is less than the cutoff distance, the CNT pair is considered in contact. Due to the van der Waals repellent force, the walls of contacting CNTs are not separated by less than the  $d_{vdW}$ .

$$\tau = \begin{cases} \exp\left(-\frac{d_{vdW}}{d_{tunnel}}\right) & 0 \leq d_{ij} \leq D + d_{vdW} \\ \exp\left(-\frac{d_{ij} - d}{d_{tunnel}}\right) & D + d_{vdW} < d_{ij} \leq D + d_{cutoff} \end{cases} \quad (5)$$

Tunneling distance is obtained by  $d_{tunnel} = h/\sqrt{(8m_e \Delta E)}$  where  $m_e$  is the mass of electron,  $\Delta E$  is the height of barrier potential. By the first order Taylor expansion and using the integral  $\int_0^\infty \frac{x}{e^x + 1} dx = \frac{\pi^2}{12}$ , the asymptotic expression of Eq. (4) can be derived as depicted in Eq. (6).

$$\int_0^\infty \tau M \frac{1}{e^{\frac{E-\mu}{k_B T}} + 1} dE \approx \int_0^\mu \tau M dE + \frac{\pi^2}{6} (k_B T)^2 \frac{d[\tau M]}{dE} \quad (6)$$

To derive a concise formula to estimate the tunneling resistance, we consider the asymptotic behavior of Eq. (6) using Sommerfeld expansion with respect to the temperature  $T$ .

$$I = \frac{2e}{h} \left\{ \int_\mu^{\mu+eV} \tau M dE + \frac{\pi^2}{6} (k_B T)^2 \times \frac{d[\tau M]}{dE} \Big|_{\mu}^{\mu+eV} \right\} \quad (7)$$

Under low bias voltage  $V$ , it can be estimated that  $\int_\mu^{\mu+eV} \tau M dE \approx eVM\tau$  and  $\frac{d[\tau M]}{dE} \Big|_{\mu}^{\mu+eV} \approx eVM \frac{d\tau}{dE} \Big|_{\mu}$ . Here, the channel number  $M$  is assumed to be an integer that cannot follow a continuous change of

variable  $E$ . Then Eq. (7) is reduced to an averaged 1-D tunneling model, and the contact resistance can be evaluated by Eq. (8).

$$I = \frac{2e}{h} \left\{ \int_{\mu}^{\mu+eV} \tau M dE + \frac{\pi^2}{6} (k_B T)^2 \times \frac{e V M d^2 T}{d E^2} |\mu| \right\} \approx \frac{2e}{h} \left\{ \int_{\mu}^{\mu+eV} \tau M dE \right\} \quad (8)$$

Current carried per unit energy is equal to  $\frac{2e}{h}$  which is about 80 nA/meV. Wide conductors containing large number of tunneling points have very small tunneling resistance.

Using the tunneling probability formula Eq. (5), resistivity can be deduced from Eq. (9).

$$R_{ij} = \frac{h}{2e^2} \frac{1}{M \tau_{ij}} = \frac{h}{2e^2 M \exp\left(-\frac{d_{ij}\sqrt{8m_e\Delta E}}{h}\right)} \quad (9)$$

Here  $m_e (9.1093829 \times 10^{-31} \text{ kg})$  is the mass of electron. Multiplying  $a$  which is the area for electrons to tunnel, equal to the cross-sectional area approximated by  $\pi d^2/4$  to top and bottom of division line, tunneling resistivity between two neighboring CNTs can be achieved by Eq. (10) [35].

$$\begin{aligned} Y(s_0, t_0, s_1, t_1) &= \frac{1}{2} \|X_0(s_0, t_0) - X_1(s_1, t_1)\|^2 \\ &= \frac{1}{2} (s_0^2 + t_0^2 + s_1^2 + t_1^2) - s_0 s_1 (U_0^T \cdot U_1) - s_0 t_1 (U_0^T \cdot V_1) - t_0 s_1 (V_0^T \cdot U_1) - t_0 t_1 (V_0^T \cdot V_1) + s_0 (U_0^T \cdot \Delta) + t_0 (V_0^T \cdot \Delta) - s_1 (U_1^T \cdot \Delta) - t_1 (V_1^T \cdot \Delta) + \frac{1}{2} \|\Delta\|^2 \\ &= \frac{1}{2} p^T \begin{bmatrix} 1 & 0 & -U_0^T \cdot U_1 & -U_0^T \cdot V_1 \\ 0 & 1 & -V_0^T \cdot U_1 & -V_0^T \cdot V_1 \\ -U_0^T \cdot U_1 & -V_0^T \cdot U_1 & 1 & 0 \\ -U_0^T \cdot V_1 & -V_0^T \cdot V_1 & 0 & 1 \end{bmatrix} p + [U_0^T \cdot \Delta V_0^T \cdot \Delta - U_1^T \cdot \Delta - V_1^T \cdot \Delta] p + \frac{1}{2} \|\Delta\|^2 = \frac{1}{2} p^T Q p + f^T p + c \end{aligned} \quad (10)$$

$$R_{ij} = \frac{h^2 \cdot d_{ij} \cdot \exp\left(\frac{4\pi d_{ij}\sqrt{2m_e\Delta E}}{h}\right)}{ae^2 \sqrt{2m_e\Delta E}} \quad (11)$$

Tunneling effect happens between two CNTs when the shortest distance between them is less than the cutoff distance that is the maximum possible thickness of the polymer separating two CNTs that allows electron hopping  $d_{\text{vdW}} + d < d_{ij} < d + d_{\text{cutoff}}$ .

The shortest distance between each pair of straight CNTs are calculated to determine if the pair is in contact or not. The distance between two CNTs is calculated using the technique to calculate the distance between two skew lines. The calculation involves forming vectors along the directions of the lines and using both the cross product and the dot product. If  $i$  th and  $j$  th CNTs' vectors ( $v_i$  and  $v_j$ ) are connected by a vector  $v_{ij}$ , the minimum distance between them is defined as  $d_{ij} = \frac{\|v_{ij} \cdot (v_i \times v_j)\|}{\|v_i \times v_j\|}$ .

## 2.2. Integration of GNPs

It is well known that the electrical conductivity of CNT/GNP composites can be represented by the resistance of CNT/GNP percolating network inside the composite. GNP is assumed as a thin rectangular cube

with side length  $S$  and thickness  $t$  which its intrinsic resistivity is  $R_f = \frac{S}{t^2 \sigma_f}$ . GNPs can be found in rectangular form as declared in previous experimental studies [36,37]. The  $i$ -th GNPs can be positioned through the set of coordinates of the starting point ( $x_0^i, y_0^i, z_0^i$ ) and two nonzero arbitrary vectors passing through the starting point in which their cross product is the normal to the GNP surface. In the RVE, GNPs are randomly generated and uniformly dispersed with origin  $P_i$  and the two vectors from origin be  $U_i$  and  $V_i$  which sketches edges of rectangular GNP [3].

$$U_i = \begin{Bmatrix} u_x^i \\ u_y^i \\ u_z^i \end{Bmatrix}, V_i = \begin{Bmatrix} v_x^i \\ v_y^i \\ v_z^i \end{Bmatrix}, u_x^i, u_y^i, u_z^i, v_x^i, v_y^i = S. \text{"rand"}, v_z^i = \frac{-(u_x^i \cdot v_x^i + u_y^i \cdot v_y^i)}{u_z^i} \quad (12)$$

The symbol  $S$  is GNP side length. Points on the thin rectangular GNP are represented by Eq. (12) [38].

$$X_i = P_i + s_i U_i + t_i V_i \quad (13)$$

Here the parameters  $0 < s_i < 1$  and  $0 < t_i < 1$  are unknowns and  $\|U_i\|$  and  $\|V_i\|$  represents the length and width of thin rectangular GNP. GNP thickness added to half squared distance between two individual GNPs is defined as depicted in Eq. (13) [38,39].

$$\text{where } p = [s_0 t_0 s_1 t_1]^T, \Delta = C_0 - C_1, f = [U_0^T \cdot \Delta V_0^T \cdot \Delta - U_1^T \cdot \Delta - V_1^T \cdot \Delta] \text{ and } c = \frac{1}{2} \|\Delta\|^2.$$

Finding the minimum of the problem where  $Y$  is a function that returns a scalar and accepts the variables  $(s_0, t_0, s_1, t_1)$ , "fmincon" of MATLAB attempts to find a minimum of a scalar function of several variables, starting at an initial estimates. For minimizing the objective function, subject to the bound constrain, lower and upper bounds on individual components, instead of writing two files, objective function and bounding constrain, one file is written which contains both functions as local functions. Then the constrained minimization starts from starting point and local minimum function finds variables which satisfy the constraints. The minimum distance between a CNT,  $X_0(s_0) = P_0 + s_0 Q_0$  and a GNP,  $X_1(s_1, t_1) = P_1 + s_1 U_1 + t_1 V_1$  can be described by Eq. (14).

$$Y(s_0, s_1, t_1) = \frac{1}{2} \|X_0(s_0) - X_1(s_1, t_1)\|^2 \quad (14)$$

**Fig. 2** shows the schematic representation of the hybrid CNT/GNP nano-structure with different CNT and GNP dispersion conditions. The details of the CNT maximum orientation angle and GNP dispersion

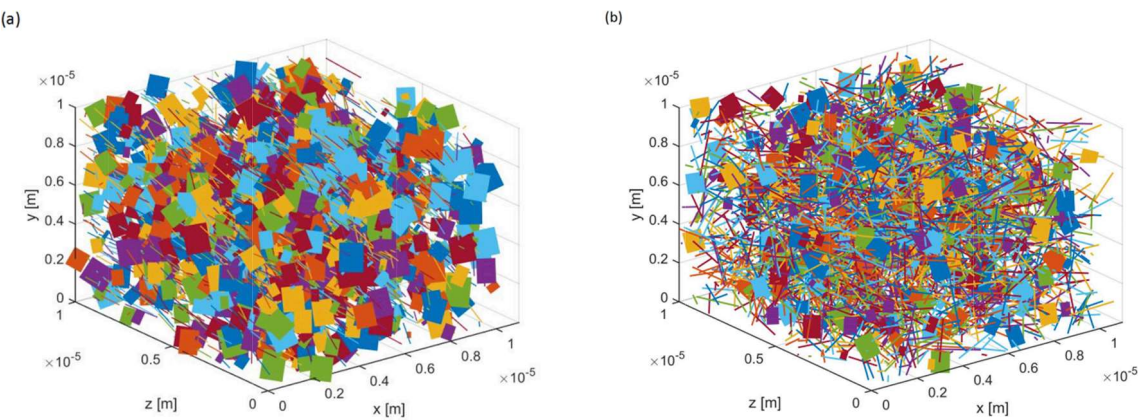


**Fig. 2.** Schematics of the nano-structure of nanocomposites with different CNT and GNP dispersion conditions.

**Table 1**  
Details of the CNTs and GNPs dimensional characteristics in the RVE.

| Schematic description | Max. CNT orientation angle (rad) |          | Volume fraction (vol.%) |     | Length (Side length) ( $\mu\text{m}$ ) |     |
|-----------------------|----------------------------------|----------|-------------------------|-----|--|-----|
|                       | $\varphi$                        | $\theta$ | CNT                     | GNP | CNT                                    | GNP |
| 2(a)                  | $\pi/6$                          | $\pi/12$ | 0.2                     | 1.2 | 2                                      | 2   |
| 2(b)                  | $\pi$                            | $\pi/2$  | 0.3                     | 0.6 | 3                                      | 1.5 |

condition are listed in **Table 1**.

The electrical resistance of a network of randomly dispersed CNTs and GNPs is known to be dominated by the tunneling of the electrons between nearby CNTs and GNPs [40]. Quantum phenomena of nearest-neighbor CNTs and GNPs interactions connecting two sides of the conductive network via transport of electron along fillers are dominant and several orders larger in magnitude than nanofillers intrinsic resistance, therefore, contact and tunneling resistances between CNTs and GNPs were preferred and the intrinsic resistance and CNTs and GNPs were ignored [41,42].

The resistivity is evaluated by recognizing the connective percolating network linking two opposite faces of RVE. Once a conductive network is found, the Dulmage-Mendelsohn decomposition method is used on the conductive network to eliminate the segments that do not participate in conducting current. Then the remaining conductive network is transformed into resistor network by calculating the resistance between the different nodes.

Passing from one CNT or GNP to another makes an increase in electrical potential. Presenting the electrical potential of the  $i$  th CNT or GNP by  $\vartheta_i$ , the current flow from  $i$  th CNT or GNP to each electrode can be demonstrated with the assembly of tunneling currents from the  $j$  th CNT or GNP to other CNTs or GNPs and from  $j$  th CNT or GNP to the two electrodes. Then, the system of equations that determines the voltage distribution over the resistor network is solved based on Kirchhoff's law [43].

$$\sum_{j=1,2}^N \frac{\vartheta_i - \vartheta_j}{R_{ij}} + \sum_{i=1}^2 \frac{\vartheta - \vartheta_j}{R_{ij}} = 0, j = 3, 4, \dots, N \quad (15)$$

Here the first term is the sum of tunneling from  $j$  th CNT or GNP to other CNTs or GNPs and the second term refers to the sum of tunneling currents from  $j$  th CNT or GNP to two electrodes. A Cholesky decomposition algorithm for sparse matrices is used to solve these matrix equations and to find the potentials. The current passing through each CNT or GNP is calculated by  $I_{ij} = (\vartheta_i - \vartheta_j)/R_{ij}$ , using Ohm's law, the conductivity is obtained  $\sigma = \sum_{\theta_L} I_{ij}$ .

**Fig. 3** demonstrates a flowchart of the steps taken to identify

percolation threshold, electrical conductivity and piezoresistivity of nanocomposite considering randomly dispersed hybrid CNT/GNP fillers with different morphologies. First, a 3D RVE of size  $L_x \times L_y \times L_z$  is generated. Next, CNTs as line segments and GNPs as rectangular platelets are randomly distributed in the 3D cube. The dimension and orientation of nanotubes and platelets are described based on random numbers. The shortest separation distance between neighboring fillers is evaluated and particles with inter-particle distance less than the tunneling cutoff distance are assumed electrically connected. With existence of at least one conductive path, the electrical conductivity of the RVE is computed in terms of resistance proportional to the separation distance. With the construction of other conduction paths, Kirchhoff's current and Ohm's law are used with the incomplete Cholesky conjugate gradient method to predict the overall resistance of the RVE. Later, to study the piezoresistivity of the nanocomposite, a strain is applied to the RVE and the new geometrical characteristics of the RVE and fillers updated coordinates and positions are defined. The obtained new configuration of the electronic band structure is used to detect the new percolating CNT-GNP networks in the RVE leading to calculation of the electrical resistance. The new resistance of the RVE at a fixed strain is compared to the resistance of the unstrained RVE to compute piezoresistivity. Then, Strain is incremented at each step, and the procedure is repeated.

### 2.3. Piezoresistivity

In this study the piezoresistivity of percolated RVE is modeled. Tensile strains were applied to the RVE and the change in electrical resistance was observed. The formulation for the 3D modeling of piezoresistivity is done by assuming a perfect mechanical coupling between the matrix, CNTs and GNPs [14]. Therefore, any applied strain will result in the deformation of each CNT and GNP and in the change of their orientations. When the CNT/GNP polymer composite is under an incremental uniaxial strain  $\Delta\epsilon$  along the Z-axis, the coordinates of the center point of the  $i$  th CNT segment distributed in the RVE  $(\bar{x}_c^i, \bar{y}_c^i, \bar{z}_c^i)$  will become [44,45].

$$\left( \bar{x}_c^i, \bar{y}_c^i, \bar{z}_c^i \right) = (x_c^i(1 - \nu\Delta\epsilon), y_c^i(1 - \nu\Delta\epsilon), z_c^i(1 + \Delta\epsilon)) \quad (16)$$

Where  $(\bar{x}_c^i, \bar{y}_c^i, \bar{z}_c^i)$  is the updated coordinates of the center point of the  $i$  th CNT segment and  $\nu$  is the Poisson's ratio. After strain is applied, a new state of CNTs will happen in the RVE and more CNTs tend to be aligned along the stretching direction. The coordinated of starting and ending points of the  $i$ -th CNT after strain are expressed as drafted in Eq. (17).

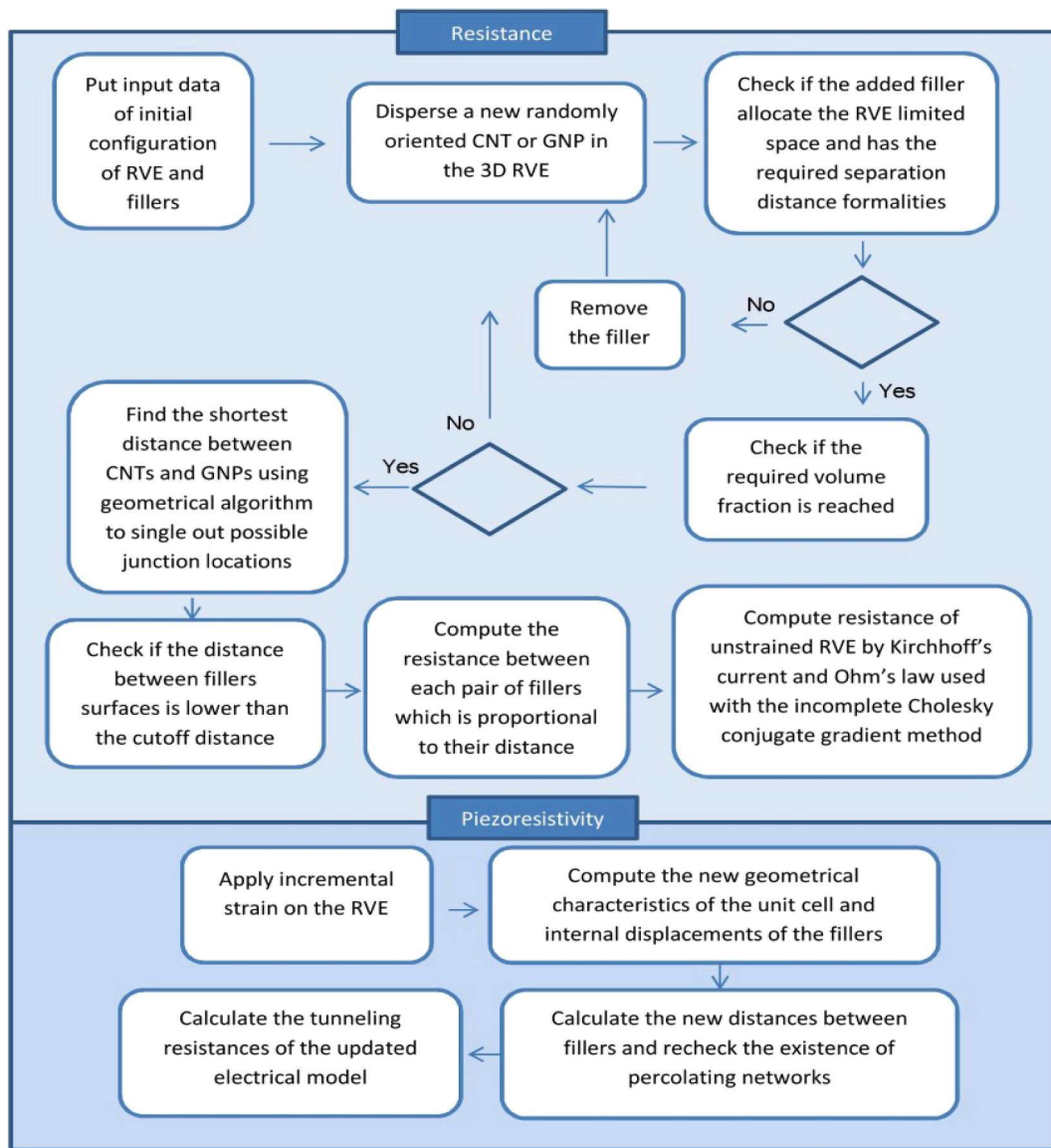


Fig. 3. Flowchart of different calculation steps of Monte Carlo simulation based on the present methodology.

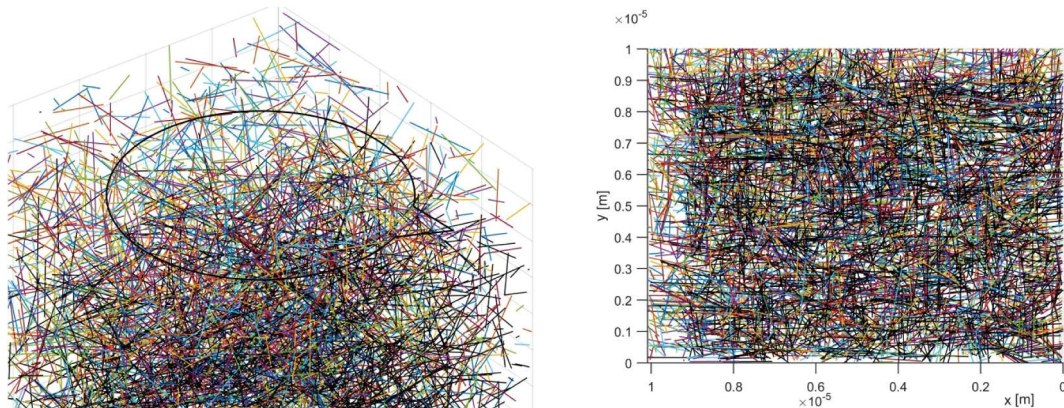


Fig. 4. Schematic of the CNT nano-structure change with the strain.

**Table 2**  
CNT nanostructure change with the strain.

| RVE Condition | Mean X position (μm) | Mean Y position (μm) | Mean Z position (μm) | Mean orientation angle (rad) |
|---------------|----------------------|----------------------|----------------------|------------------------------|
| Unstrained    | 4.9332               | 4.9999               | 5.0209               | 1.5688                       |
| Strained      | 4.6612               | 4.6885               | 5.6553               | 1.4317                       |

$$\bar{x}_0^i = \bar{x}_c^i - \left\{ \bar{x}_c^i - x_0^i(1 - \nu\Delta\varepsilon) \right\} \times \begin{pmatrix} l_i \\ \bar{l}_i \end{pmatrix},$$

$$\bar{y}_0^i = \bar{y}_c^i - \left\{ \bar{y}_c^i - y_0^i(1 - \nu\Delta\varepsilon) \right\} \times \begin{pmatrix} l_i \\ \bar{l}_i \end{pmatrix},$$

$$\bar{z}_0^i = \bar{z}_c^i - \left\{ \bar{z}_c^i - z_0^i(1 + \Delta\varepsilon) \right\} \times \begin{pmatrix} l_i \\ \bar{l}_i \end{pmatrix},$$

$$\bar{x}_1^i = \bar{x}_c^i + \left\{ x_1^i(1 - \nu\Delta\varepsilon) - \bar{x}_c^i \right\} \times \begin{pmatrix} l_i \\ \bar{l}_i \end{pmatrix},$$

$$\bar{y}_1^i = \bar{y}_c^i + \left\{ y_1^i(1 - \nu\Delta\varepsilon) - \bar{y}_c^i \right\} \times \begin{pmatrix} l_i \\ \bar{l}_i \end{pmatrix},$$

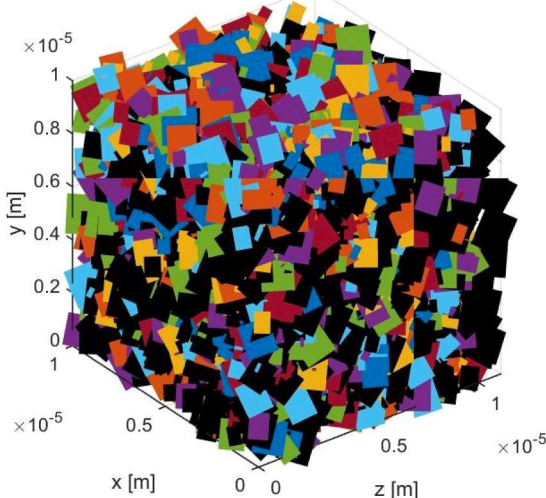
$$\bar{z}_1^i = \bar{z}_c^i + \left\{ z_1^i(1 + \Delta\varepsilon) - \bar{z}_c^i \right\} \times \begin{pmatrix} l_i \\ \bar{l}_i \end{pmatrix} \quad (17)$$

The locations of CNT intersections will transform after strain. Fig. 4 shows a schematic representation of the CNT polymer strained composite (10% of strain) in the Z-direction which CNTs in black are moved by strain. The details of CNTs' nanostructure change with strain are drafted in Table 2.

Following the re-orientation model, the change in GNP position is considered here. With tensile strain in the Z-direction, the starting point  $P_i$  of the  $i$  th GNP moves transnationally in accordance with the strain and the Poisson's ratio, as depicted in Eq. (18) [46].

$$\bar{P}_x^i = P_x^i(1 - \nu\Delta\varepsilon), \bar{P}_y^i = P_y^i(1 - \nu\Delta\varepsilon), \bar{P}_z^i = P_z^i(1 + \Delta\varepsilon) \quad (18)$$

Where  $i$  is the index of  $i$  th GNP. The updated vectors from origin are



described in Eq. (19) [47].

$$\bar{U}_i = \begin{Bmatrix} u_x^i(1 - \nu\Delta\varepsilon) \\ u_y^i(1 - \nu\Delta\varepsilon) \\ u_z^i(1 + \Delta\varepsilon) \end{Bmatrix} \quad (19)$$

$$\bar{V}_i = \begin{Bmatrix} v_x^i(1 - \nu\Delta\varepsilon) \\ v_y^i(1 - \nu\Delta\varepsilon) \\ v_z^i(1 + \Delta\varepsilon) \end{Bmatrix}$$

Eventually, the separation distance of a pair of rectangular GNPs is calculated by Eq. (13).

The change in the electrical resistance of the composite due to the mechanical deformation can be expressed as depicted in Eq. (20) [12].

$$\frac{\Delta R}{R} = \frac{R_{\text{new}} - R}{R} = \frac{R_{\text{new}}}{R} - 1 \quad (20)$$

Here  $R$  and  $R_{\text{new}}$  are the electrical resistances of the undeformed and deformed composites, respectively. And  $\Delta R$  is the corresponding change of the electrical resistance of the nanocomposite caused by mechanical deformation [31]. Fig. 5 shows the schematic representation of GNP polymer strained composite (10% of strain) in the Z-direction where GNPs in black are transformed by strain.

### 3. Results and discussion

To demonstrate the validity of the proposed single-step Monte Carlo approach, the comparison between the calculated electrical conductivity and the experimental data of GNP composite filled with a specific CNT volume fraction is done. The experimental data was obtained from the Liu et al. [48], Al-saleh [49], Gao et al. [50], Stankovic et al. [51], and Qi et al. [52]. The composite tested by them used different volume fractions of fillers but with approximately similar GNP and CNT properties. In the calculation, the two important parameters are taken as  $\Delta E = 3\text{eV}$  and  $d_{\text{cutoff}} = 1.4\text{nm}$ . To reduce the computational cost, the dimension of the unit cell was set to  $10 \times 10 \times 10\mu\text{m}^3$ , which has been estimated to be large enough for an reliable prediction. It is evident from Fig. 6(a) that there is a good agreement between the calculated and experimentally measured electrical conductivity of the composite. There are some discrepancies related to uniform dispersion state assumed in the model while most experiments cannot fabricate composite with filler uniform dispersion. Fig. 6(a) also shows that the values of the electrical conductivity of the nanocomposite increased several orders of

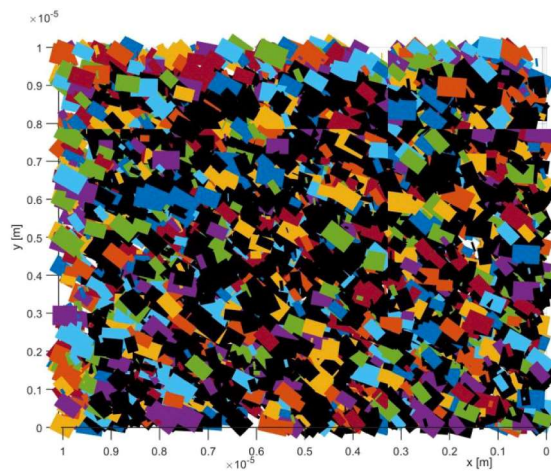


**Fig. 5.** Schematic of the GNP nano-structure variation with the strain.

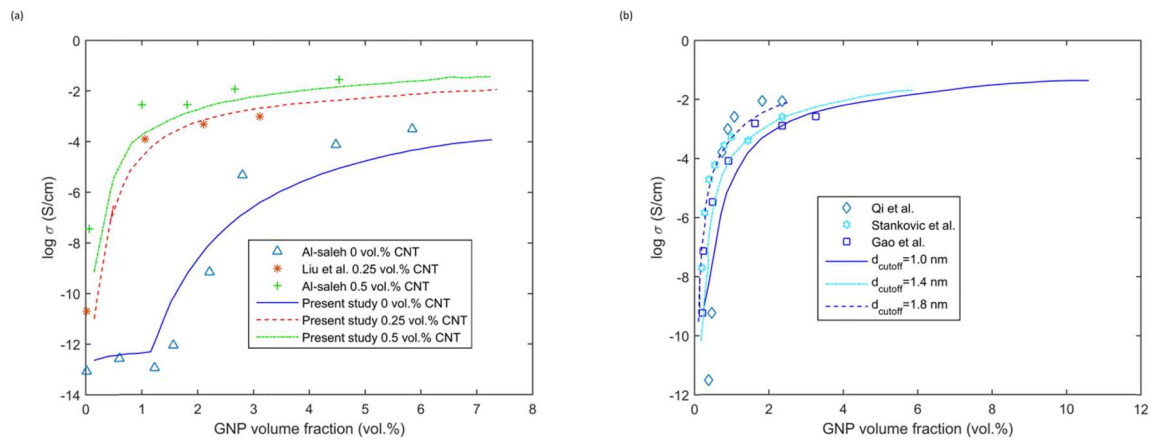


**Fig. 6.** Comparison of present study predictions and (a) experimental data [48,49], and (b) experimental data [50–52].

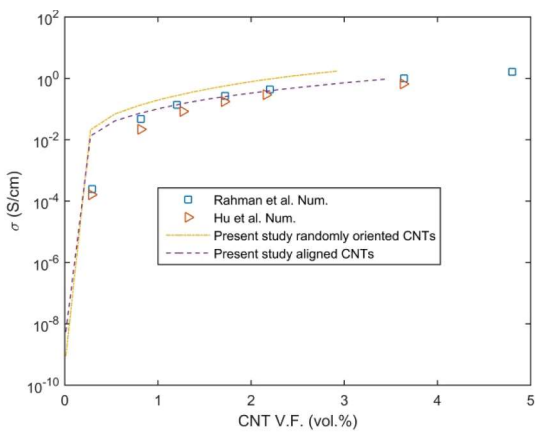


**Fig. 7.** Comparison between the predicted results of the analytical model and the numerical estimations [26,53].

**Table 3**  
Dimensional and electrical properties of CNT and GNP [9,28,47,49].

| Property                               | CNT    | GNP    |
|--|--------|--------|
| Intrinsic conductivity (S/m)           | 10,000 | 50,000 |
| Length (Side length) ( $\mu\text{m}$ ) | 4      | 3      |
| Diameter (Thickness) (nm)              | 10     | 30     |
| Height of barrier potential (eV)       | 4      | 4      |
| Cutoff distance (nm)                   | 1.4    | 1.4    |

magnitude within a small volume fraction range of GNP. In order to see the overall electrical conductivity dependence on the value of cutoff distance, Fig. 6(b) shows predicted effective electrical conductivity of model in comparison with the experimental data of GNP composite with 0 vol% of CNT. The small discrepancy may be attributed to the assumptions made, such as cutoff distance, fixed side length and thickness of GNPs. From Fig. 6(b), it can be seen that for a composite with a fixed volume fraction, the increase in the cutoff distance marginally increases the electrical conductivity. Such small dependence may partly relate to tunneling which decays exponentially with cutoff distance and exponential behavior of  $\tau$  make the compensations for large cutoff distance.

To further verify the model's electrical conductivity predictions, the model results of CNT/polymer nanocomposite are compared with Rahman et al. [26] and Hu et al. [53] numerical studies predictions. Fig. 7 demonstrates that the electrical conductivities predicted by model agree well with the numerical studies predictions.

Multiple RVEs filled with CNTs and GNPs with volume fraction

ranging from 0.1% to 15% are created to examine the effect of various parameters on the electrical conductivity and piezoresistivity. The material properties of CNT and GNP are depicted in Table 3 which are derived based on previous numerical and experimental studies.

In order to predict the effects of different parameters on the conductivity of nanocomposite, the electrical conductivity is plotted with respect to GNP volume fraction. The electrical conductivity of hybrid nanocomposite with different CNT aspect ratios is shown in Fig. 8(a) as a function of GNP volume fraction. Aspect ratio  $l/d$  is an important parameter that combines the influence of the length and diameter of CNT into one parameter attributed to effective length. Fig. 8(a) demonstrates that the conductive properties of the nanocomposite are closely related to the aspect ratio of CNT and electrical conductivity increases with aspect ratio because larger aspect ratio indicates longer conductive pathways and more interactions. Whereas, the reduction of effective length by lower aspect ratio would not be beneficial for the formation of effective conductive networks by reducing the number of inter-tube tunneling contacts along a conductive path. This reveals that larger aspect ratio is mainly beneficial for the synergy arising from the hybrid fillers which helps the average separation distance falls in the suitable theoretical range  $< 1.4$  nm for electron hopping. Fig. 8(b) presents the effects of the GNP side length on the electrical conductivity of the hybrid nanocomposite. Obviously, the GNP side length has a significant effect of the percolation threshold while its influence on the overall electrical conductivity extenuates at higher volume fraction. This finding is understandable because the effect of side length of the GNP is prominent when GNPs are sparsely dispersed and further increasing the volume fraction can attenuate this effect. In addition, the higher probability of the formation of conductive networks related to electron hopping at higher volume fraction contributes to this decreasing trend.

Fig. 9 shows the effect of CNT orientation and heights of barrier potential on the electrical conductivity of nanocomposite as a function of GNP volume fraction. Randomly oriented CNTs relate to maximum orientation angle and aligned CNTs refer to minimum orientation angle. Results show that the percolation happens earlier in nanocomposites with randomly oriented CNTs, indicating that the electrical conductivity can be effectively enhanced by distributing CNTs in all possible directions. The extent of interactions between the nanofillers and matrix polymer in the nanocomposite is significantly controlled by the interfacial area and channel length. This means that highly aligned CNTs would not be beneficial to provide a highly conductive network due to the weak interactions between themselves. Whereas, randomly oriented CNTs lead to an exceptionally large interfacial area of nanocomposite where many conductive paths exist accompanied with huge interconnections. As shown in Fig. 9(b), the dependence of electrical conductivity on potential barrier height provides significant insights

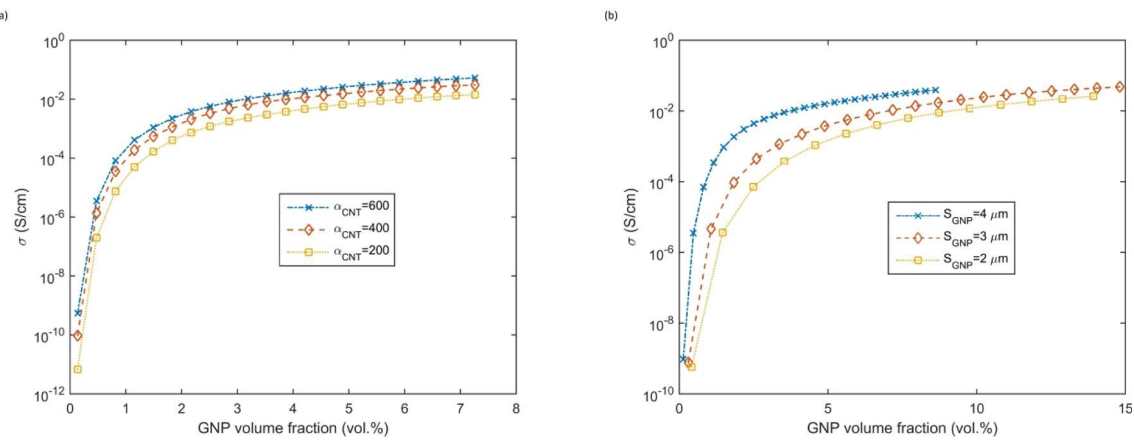


**Fig. 8.** Predicted electrical conductivity of hybrid nanocomposite with 0.25 vol% CNT versus the GNP volume fraction for different (a) CNT aspect ratios (b) GNP side lengths.

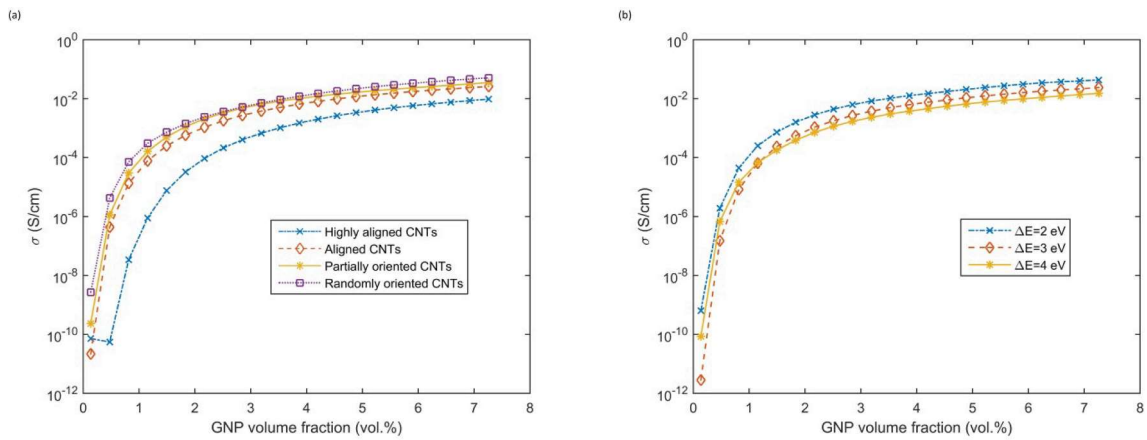


**Fig. 9.** Predicted electrical conductivity of hybrid nanocomposite versus the GNP volume fraction for different (a) CNT orientations (b) heights of barrier potential.

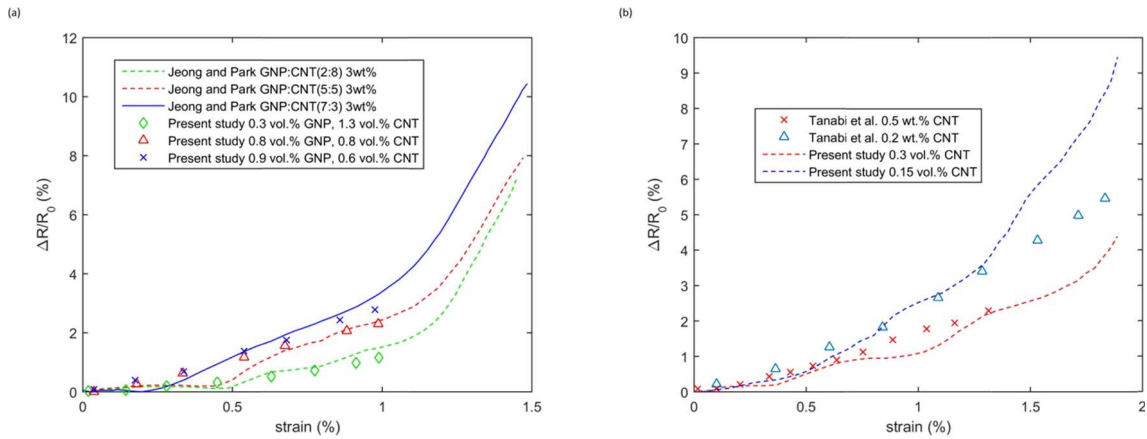


**Fig. 10.** Comparison of piezoresistivity predicted by the model for (a) CNT/GNP nanocomposite with experimental data [54], and (b) CNT nanocomposite with experimental data [55].

into the effect of work function difference between fillers and polymer. Based on percolation theory, formation of continuous network among fillers can be achieved if electron could transport between CNTs. Moreover, the insulating polymer thickness between crossing CNTs plays a significant role in the tunneling resistance which depends on height of barrier potential. Therefore, the decreasing height of barrier potential allows more CNTs to be connected in order to form the

conductive paths. The surface area related to the incorporation of more filler in the percolation network led to this higher electrical conductivity.

The CNT/GNP hybrid nanocomposite is employed for the purpose of theoretically predicting the piezoresistivity obtained in previous experiments. Comparisons between the analytical predictions and the experimental data of Jeong and Park [54] are shown in Fig. 10(a) with

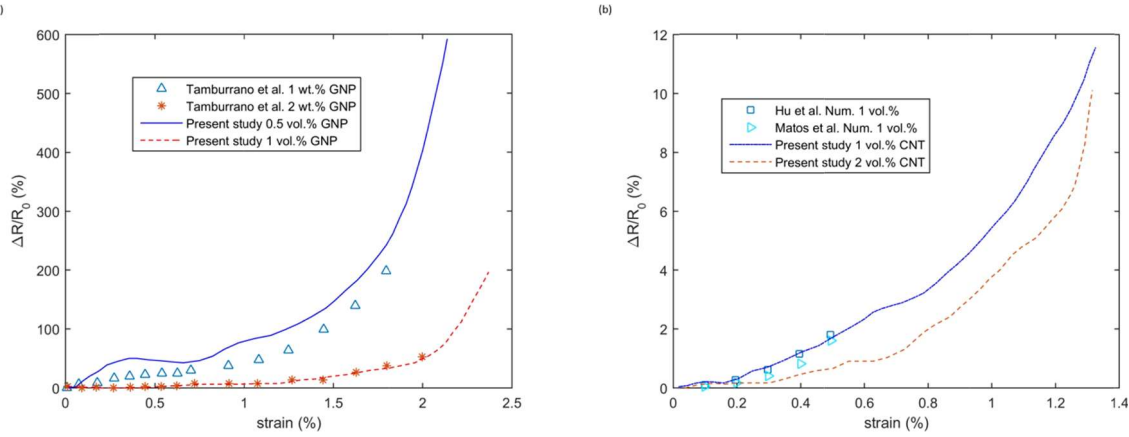


**Fig. 11.** Comparison of piezoresistivity predicted by the model for (a) GNP polymer nanocomposite with experimental data [56], and (b) CNT polymer nanocomposite with numerical results [58,59].

different volume fraction ratios of CNT/GNP. Referred to experimental data, the predicted response of the material is almost linear regarding relatively low strains in accordance with the model predictions. However, the model predicts an initial non-linear decrease of the resistance change ratio versus strain due to the variations of the locations of CNTs and GNPs in the strained RVE. New paths may form and existing paths may break due to the incremental strain of 0.05% at each time step inflicted on the RVE. In the beginning of the curve, it seems that the average number of distorted paths overweight the average number of formed paths. In addition, at low strain, the distances of adjacent CNTs were short and the conductive network still could keep the stable state under small deformation. Later, model predicted that the resistance exponentially increased with applied strain. This phenomenon is related to the destruction of the conductive network inside the polymer composite and the reduction of percolated CNT paths. In all cases, a very good agreement can be noted between model predictions and experimental data, indicating the capability of the model to predict the piezoresistivity behavior. Fig. 10(b) shows piezoresistivity of nanocomposite for different CNT volume fractions in comparison with experimental data of Tanabi et al. [55]. Randomly oriented CNTs had an average diameter of 10 nm and an average length of 1.5  $\mu\text{m}$ . Fig. 10(b) illustrates that there is a good agreement between the model predictions and the experimental data. Fig. 10(b) also demonstrates that the change in resistance is mild with higher CNT volume fraction related to more overlaps generated among CNTs which is understandable because when the CNTs are highly populated in any direction then any change in the strain will change both the linear and angular distance between the CNT pairs.

To investigate the validity of the proposed model, the piezoresistivity predictions are compared with Tamburrano et al. [56] experimental data. The GNP's wt.% can be converted to the GNP's vol.% considering GNP's density ( $2.1 \text{ g/cm}^3$ ) and polymer's density ( $1.05 \text{ g/cm}^3$ ) [57]. Fig. 11(a) demonstrates that the present model predictions match well with the experimental data reflecting that, at the same strain, differences in scattered GNPs' volume fractions lead to different resistance change ratios. Moreover, at small strains, the mean inter-platelets separation distance varies due to the improved in-plane alignment of high aspect ratio GNPs toward better electrical conductivity. At much higher strains, the conductive pathways are broken due to increased separation distance of aligned GNPs and the nanocomposite becomes more resistive.

To further exhibit the predictability of the analytical model, another comparison between the proposed model and other numerical studies (Matos et al. [58] and Hu et al. [59]) are conducted. Fig. 11(b) shows the predicted resistance change ratio versus strain for an RVE with size of  $15 \mu\text{m}$ , containing 1 and 2 vol% of CNTs. CNT's average length and diameter are  $5 \mu\text{m}$  and 50 nm. From Fig. 11(b) it can be noted that there is a small discrepancy between the analytical results derived from the current theoretical model and numerical studies. The discrepancy is due to the consideration of the different set-ups in model establishments such as different dispersion states and structures of CNTs. This is due to the fact that non-uniformly dispersed curved CNTs would experience a greater change in resistance compared with uniformly dispersed straight CNTs for the same volume fraction.

In the following, parametrical studies are carried out on the effect of different parameters on the theoretical predictions of piezoresistivity. Fig. 12(a) gives the resistance change of the nanocomposite under the

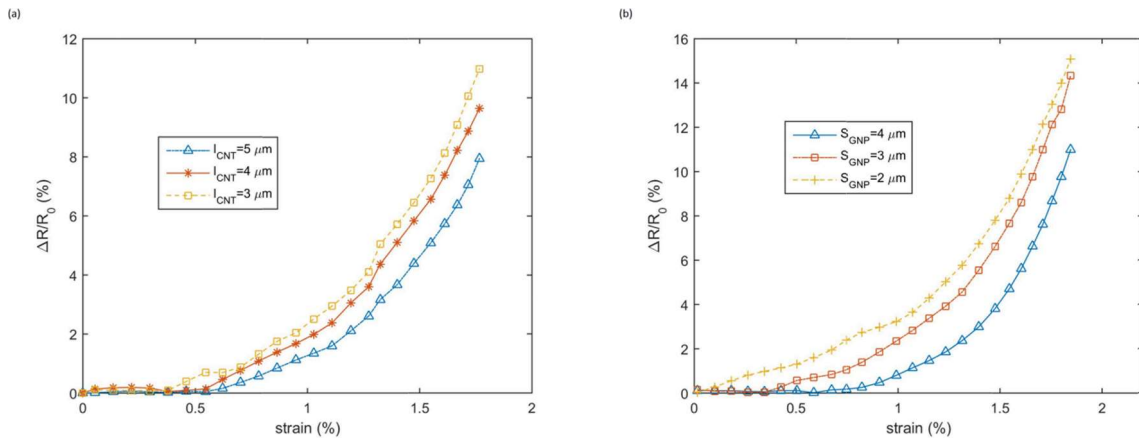


**Fig. 12.** Piezoresistivity of nanocomposite with different (a) CNT lengths and (b) GNP side lengths.

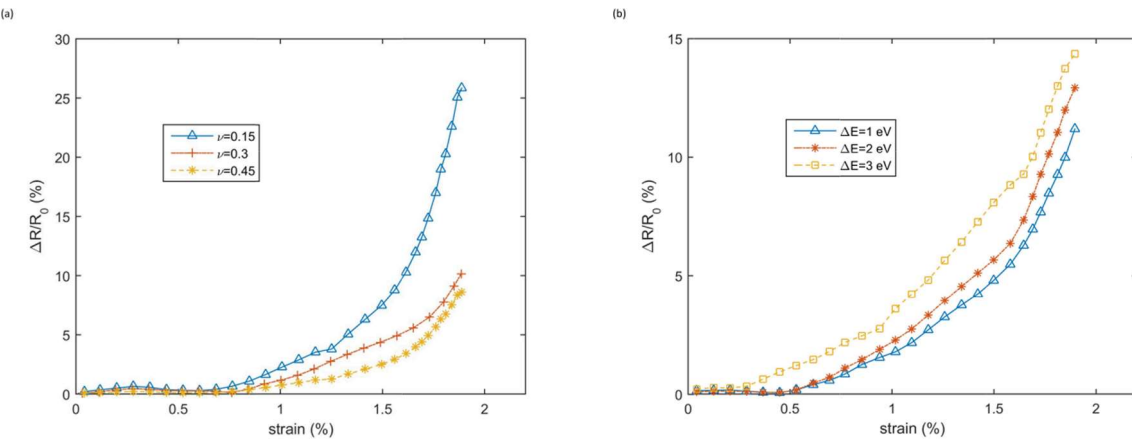


**Fig. 13.** Piezoresistivity of nanocomposite with different (a) Poisson's ratios and (b) heights of barrier potential.

applied strain for different CNT lengths while CNT diameter is kept constant at 10 nm. Considering a larger  $\Delta R/R_0$  as higher sensitivity, Fig. 12(a) exhibits that the piezoresistivity is more sensitive with shorter CNTs. This reveals that nanocomposites with shorter CNTs are more susceptible to the breakdown of conductive networks. This is understandable as the increase in CNT length could increase the overlap ratio between CNTs which leads to longer network length affecting the electrical response of the nanocomposite coming from the exponential dependence of the resistance change ratio versus strain. Fig. 12(b) shows the influence of GNP side length on piezoresistivity. Fig. 12(b) demonstrates that resistance change ratio increased almost linearly with the strain at the beginning following by an exponential increase. As expected from theory, inter-particle distance increases extremely with further increment of the gap between fillers since a higher deformation span influences the network of fillers inside the polymer more widely. Fig. 12(b) also suggests that the resistivity of the nanocomposite with smaller GNP side length is more sensitive to stretching because GNPs with larger side length appear to have a permanent contribution by bridging and promoting electron tunneling. In this case, the average separation distance easily falls in the analytical range  $< 1.4$  nm where the lower limit is imposed due to van der Waals interactions and upper limit is enforced by distance available for the electric conduction between two platelets. Also, the specific surface area of the GNP is much larger as a natural consequence of the larger side length which leads to physical contact between platelets to form conductive pathways and prohibit the breakdown of conductive networks. This again emphasizes the importance of the low average separation distance provided by large surface area for tunneling-type contact between adjacent platelets.

Fig. 13 plots the measured resistance change  $\Delta R$  normalized by the

initial resistance  $R_0$ , as a function of the tensile strain for different Poisson's ratios and heights of barrier potential. It is assumed that the effect of filler volume fraction and orientation on the Poisson's ratio is negligible. Fig. 13(a) shows that the piezoresistivity of the hybrid nanocomposite drastically changes with Poisson's ratio. This suggests the transverse motion effect that nullifies part of the strained CNTs transportation in displacement direction. The huge difference between the curves is attributed to the morphological structure of nanocomposites with different Poisson's ratios. Isotropic dispersion promotes inter-filler connection through contact, allowing the formation of continuous percolated pathways while anisotropic dispersion leads to desolating effects. As stated earlier, the condition for a charge to pass over an energy barrier with a given potential is to have the energy equal or greater than the barrier. Height of barrier potential indicates this dependency and affects the probability for a charge to pass through a potential barrier. Fig. 13(b) plots the resistance change ratio with strain for different heights of barrier potential. The decrease of sensitivity by increase in the height of barrier potential indicates the drawback of the insulating layer's potential barrier. This is quite interesting, since charge carriers choose the lowest resistance path possible through the nanocomposite and electrical conductivity network is mainly attributed to the electron hopping.

Fig. 14 shows the strain dependence of resistance change ratio for various volume fractions of CNTs and GNPs. Fig. 14(a) demonstrates that for a given level of strain, the resistance change ratios are lower when CNT volume fraction is higher. This result reflects that the previous consideration that network sparseness led to larger deformation of percolating network was true. Fig. 14(a) also demonstrates that the curves start to fluctuate from beginning due to updated fillers positions

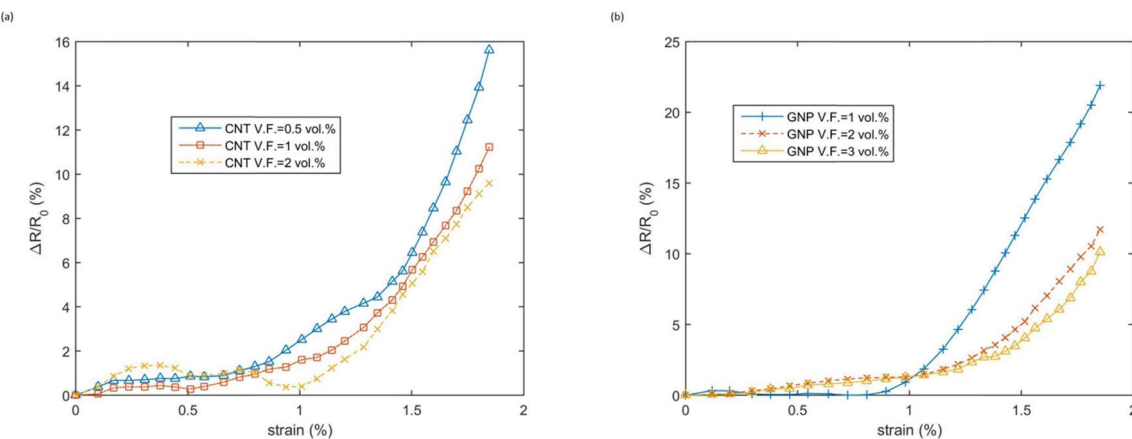


**Fig. 14.** Piezoresistivity of nanocomposite with different (a) CNT volume fractions and (b) GNP volume fractions.

and recalculated tunneling resistance between them. At percolation threshold, where fillers are separated with critical distances, strain has remarkable effect on the decrease or increase of the number of CNTs' contacts which creates high sensitivity related to the distortion or formation of percolation paths. This formation of conductive pathways in small strain is more specifically related to the straightening of individual disordered GNPs to evolved ordered aligned ones which decrease the efficacy of conducting pathways in primary increments of strain. Fig. 14(b) shows that the piezoresistivity substantially depends on GNP volume fraction and suggests that the resistivity of the composite with lower GNP volume fraction is more sensitive to stretching. This indicates that composite has higher sensitivity when a small number of conductive networks exist in nanocomposites. Fig. 14(b) also demonstrates a special tendency of the curve with lowest GNP volume fraction, which is related to the setup of the model and it seems that the number of distorted paths is equal to the number of paths created for the small strain. This is stemming from the fact that at small strains, the mean inter-particle distance may decrease due to the rotation of the fillers that are out of order, leading to better arrangement and reduced resistivity, whereas at higher strain, the in-plane inter-particle separation distance of aligned GNPs increases so the conductive paths are broken and the nanocomposite becomes more resistive. It seems that at earlier stage of strain range these two competing considerations are balanced.

#### 4. Conclusion

The 3D Monte Carlo simulation was used to investigate the electrical conductivity and piezoresistivity of CNT/GNP polymer nanocomposite using percolation network model. The analytical model has been validated by experimental data published in the literature for both electrical conductivity and piezoresistivity of hybrid nanocomposite. The study results showed that the electrical conductivity is dominated by CNT/GNP quantum tunneling influenced by cutoff distance. The influences of height of barrier, CNT's orientation, volume fraction and dimensions and GNP side length on electrical conductivity and piezoresistivity were studied. Results showed that the conductivity of composite can be effectively enhanced by increasing CNT aspect ratio, orientation angle and GNP side length. Parametric studies revealed that the increase in height of barrier potential led to a decrease of electrical conductivity and more sensitive piezoresistivity. It was also indicated that the increase in Poisson's ratio, enabled CNTs to be more aligned along the stretching direction, which decreased the piezoresistive sensitivity while a higher CNT/GNP volume fraction led to less sensitivity. Although, this work has shown success in predicting the effect of different parameters on the electrical conductivity and piezoresistivity of CNT/GNP polymer nanocomposite, its applicability in a wider scenario, especially at a relatively high CNT volume fraction is limited because the current model does not take the agglomeration effects and distortion of CNT into account.

#### CRediT authorship contribution statement

**M. Haghgoor:** Methodology, Software, Formal analysis, Investigation, Writing – original draft, Writing – review & editing. **R. Ansari:** Validation, Resources, Writing – review & editing, Supervision. **M.K. Hassanzadeh-Aghdam:** Conceptualization, Data curation, Writing – original draft, Visualization.

#### Declaration of Competing Interest

The authors declare that they have no known competing financial interests or personal relationships that could have appeared to influence the work reported in this paper.

#### References

- [1] Zhao H, Bai J. Highly sensitive piezo-resistive graphite nanoplatelet–carbon nanotube hybrids/polydimethylsiloxane composites with improved conductive network construction. *ACS Appl Mater Interfaces* 2015;7(18):9652–9.
- [2] Xiang D, Zhang X, Harkin-Jones E, Zhu W, Zhou Z, Shen Y, et al. Synergistic effects of hybrid conductive nanofillers on the performance of 3D printed highly elastic strain sensors. *Compos A Appl Sci Manuf* 2020;129:105730. <https://doi.org/10.1016/j.compositesa.2019.105730>.
- [3] Maiti S, Khatua BB. Graphene nanoplate and multiwall carbon nanotube–embedded polycarbonate hybrid composites: High electromagnetic interference shielding with low percolation threshold. *Polym Compos* 2016;37(7):2058–69.
- [4] Morales P, Moyanova S, Pavone I, Fazi L, Mirabile Gattia D, Rapone B, et al. Self-grafting carbon nanotubes on polymers for stretchable electronics. *The European Physical Journal Plus* 2018;133(6). <https://doi.org/10.1140/epjp/i2018-12040-0>.
- [5] Xiang D, Wang L, Zhang Q, Chen B, Li Y, Harkin-Jones E. Comparative study on the deformation behavior, structural evolution, and properties of biaxially stretched high-density polyethylene/carbon nanofiller (carbon nanotubes, graphene nanoplatelets, and carbon black) composites. *Polym Compos* 2018;39(S2):E909–23.
- [6] Rathi A, Kundalwal SI. Mechanical and fracture behavior of MWCNT/ZrO<sub>2</sub>/epoxy nanocomposite systems: Experimental and numerical study. *Polym Compos* 2020;41(6):2491–507.
- [7] Xiang D, Wang L, Tang Y, Harkin-Jones E, Zhao C, Li Y. Processing-property relationships of biaxially stretched binary carbon nanofiller reinforced high density polyethylene nanocomposites. *Mater Lett* 2017;209:551–4.
- [8] Chen Q, Xiang D, Wang L, Tang Y, Harkin-Jones E, Zhao C, et al. Facile fabrication and performance of robust polymer/carbon nanotube coated spandex fibers for strain sensing. *Compos A Appl Sci Manuf* 2018;112:186–96.
- [9] Perets Y, Aleksandrovych L, Melnychenko M, Lazarenko O, Vovchenko L, Matzui L. The electrical properties of hybrid composites based on multiwall carbon nanotubes with graphite nanoplatelets. *Nanoscale Res Lett* 2017;12(1):1–10.
- [10] Du J, Zhao L, Zeng Y, Zhang L, Li F, Liu P, et al. Comparison of electrical properties between multi-walled carbon nanotube and graphene nanosheet/high density polyethylene composites with a segregated network structure. *Carbon* 2011;49(4):1094–100.
- [11] Li C, Thostenson ET, Chou T-W. Dominant role of tunneling resistance in the electrical conductivity of carbon nanotube–based composites. *Appl Phys Lett* 2007;91(22):223114. <https://doi.org/10.1063/1.2819690>.
- [12] Alig I, Skipa T, Lellingen D, Bierdel M, Meyer H. Dynamic percolation of carbon nanotube agglomerates in a polymer matrix: comparison of different model approaches. *physica status solidi (b)* 2008;245(10):2264–2267.
- [13] Xiang D, Wang L, Tang Y, Harkin-Jones E, Li Y. Effect of phase transitions on the electrical properties of polymer/carbon nanotube and polymer/graphene nanoplatelet composites with different conductive network structures. *Polym Int* 2018;67(2):227–35.
- [14] Kundalwal SI, Rathi A. Improved mechanical and viscoelastic properties of CNT-composites fabricated using an innovative ultrasonic dual mixing technique. *Journal of the Mechanical Behavior of Materials* 2020;29(1):77–85.
- [15] Kundalwal SI. Review on micromechanics of nano-and micro-fiber reinforced composites. *Polym Compos* 2018;39(12):4243–74.
- [16] Wang X, Meng Si, Tebyetekerwa M, Li Y, Pionteck J, Sun B, et al. Highly sensitive and stretchable piezoresistive strain sensor based on conductive poly(styrene-butadiene-styrene)/few layer graphene composite fiber. *Compos A Appl Sci Manuf* 2018;105:291–9.
- [17] Spinelli G, Lamberti P, Tucci V, Vertuccio L, Guadagno L. Experimental and theoretical study on piezoresistive properties of a structural resin reinforced with carbon nanotubes for strain sensing and damage monitoring. *Compos B Eng* 2018;145:90–9.
- [18] Oliva-Avilés AI, Avilés F, Seidel GD, Sosa V, Seidel Gt, Sosa V: On the contribution of carbon nanotube deformation to piezoresistivity of carbon nanotube/polymer composites. *Compos B Eng* 2013;47:200–6.
- [19] Lu S, Tian C, Wang X, Chen D, Ma K, Leng J, et al. Health monitoring for composite materials with high linear and sensitivity GnP/epoxy flexible strain sensors. *Sens Actuators, A* 2017;267:409–16.
- [20] Zhang X, Xiang D, Zhu W, Zheng Y, Harkin-Jones E, Wang P, et al. Flexible and high-performance piezoresistive strain sensors based on carbon nanoparticles@polyurethane sponges. *Compos Sci Technol* 2020;200:108437. <https://doi.org/10.1016/j.compscitech.2020.108437>.
- [21] Xiang D, Wang L, Tang Y, Harkin-Jones E, Zhao C, Wang P, et al. Damage self-sensing behavior of carbon nanofiller reinforced polymer composites with different conductive network structures. *Polymer* 2018;158:308–19.
- [22] Pech-Pisté R, Cen-Puc M, Balam A, May-Pat A, Avilés F. Multifunctional sensing properties of polymer nanocomposites based on hybrid carbon nanostructures. *Mater Today Commun* 2020;25:101472. <https://doi.org/10.1016/j.mtcomm.2020.101472>.
- [23] Namilae S, Li J, Chava S. Improved piezoresistivity and damage detection application of hybrid carbon nanotube sheet-graphite platelet nanocomposites. *Mech Adv Mater Struct* 2019;26(15):1333–41.
- [24] Ke K, Yue L, Shao H, Yang M-B, Yang W, Manas-Zloczower I. Boosting electrical and piezoresistive properties of polymer nanocomposites via hybrid carbon fillers: a review. *Carbon* 2021;173:1020–40.
- [25] Li J, Fang L, Sun B, Li X, Kang SH. Recent progress in flexible and stretchable piezoresistive sensors and their applications. *J Electrochem Soc* 2020;167(3):037561.

- [26] Rahman R, Servati P. Effects of inter-tube distance and alignment on tunnelling resistance and strain sensitivity of nanotube/polymer composite films. *Nanotechnology* 2012;23(5):055703. <https://doi.org/10.1088/0957-4484/23/5/055703>.
- [27] Wang Z, Ye X. A numerical investigation on piezoresistive behaviour of carbon nanotube/polymer composites: mechanism and optimizing principle. *Nanotechnology* 2013;24(26):265704. <https://doi.org/10.1088/0957-4484/24/26/265704>.
- [28] Feng C, Jiang L. Micromechanics modeling of bi-axial stretching effects on the electrical conductivity of CNT-polymer composites. *Int J Appl Mech* 2015;07(01):1550005. <https://doi.org/10.1142/S1758825115400050>.
- [29] Souri H, Yu J, Jeon H, Kim JW, Yang C-M, You N-H, et al. A theoretical study on the piezoresistive response of carbon nanotubes embedded in polymer nanocomposites in an elastic region. *Carbon* 2017;120:427–37.
- [30] Xiang D, Zhang X, Li Y, Harkin-Jones E, Zheng Y, Wang L, et al. Enhanced performance of 3D printed highly elastic strain sensors of carbon nanotube/thermoplastic polyurethane nanocomposites via non-covalent interactions. *Compos B Eng* 2019;176:107250. <https://doi.org/10.1016/j.compositesb.2019.107250>.
- [31] Fang Y, Li L-Y, Jiang S-H. Piezoresistive modelling of CNTs reinforced composites under mechanical loadings. *Compos Sci Technol* 2021;208:108757. <https://doi.org/10.1016/j.compscitech.2021.108757>.
- [32] Tang Z-H, Li Y-Q, Huang P, Wang H, Hu N, Fu S-Y. Comprehensive evaluation of the piezoresistive behavior of carbon nanotube-based composite strain sensors. *Compos Sci Technol* 2021;208:108761. <https://doi.org/10.1016/j.compscitech.2021.108761>.
- [33] Alian AR, Kundalwal SI, Meguid SA. Multiscale modeling of carbon nanotube epoxy composites. *Polymer* 2015;70:149–60.
- [34] Zabihi Z, Araghi H. Monte Carlo simulations of effective electrical conductivity of graphene/poly (methyl methacrylate) nanocomposite: Landauer-Buttikier approach. *Synth Met* 2016;217:87–93.
- [35] Bao WS, Meguid SA, Zhu ZH, Weng GJ. Tunneling resistance and its effect on the electrical conductivity of carbon nanotube nanocomposites. *J Appl Phys* 2012;111(9):093726. <https://doi.org/10.1063/1.4716010>.
- [36] Chatterjee S, Nafezarefi F, Tai NH, Schlaggenhauf L, Nüesch FA, Chu BIT. Size and synergy effects of nanofiller hybrids including graphene nanoplatelets and carbon nanotubes in mechanical properties of epoxy composites. *Carbon* 2012;50(15):5380–6.
- [37] Baskut S, Turan S. The effect of different GNPs addition on the electrical conductivities and percolation thresholds of the SiAlON matrix composites. *J Eur Ceram Soc* 2020;40(4):1159–67.
- [38] Gbaguidi A, Namilae S, Kim D. Synergy effect in hybrid nanocomposites based on carbon nanotubes and graphene nanoplatelets. *Nanotechnology* 2020;31(25):255704. <https://doi.org/10.1088/1361-6528/ab7fcc>.
- [39] Gbaguidi A, Namilae S, Kim D. Numerical and Experimental Investigation of the Piezoresistive Behavior of Hybrid Carbon Nanotube Sheet-Graphene Nanocomposites. In: *58th AIAA/ASCE/AHS/ASC Structures, Structural Dynamics, and Materials Conference* 2017;2017:0795.
- [40] Derosa PA, Michalak T. Polymer-mediated tunneling transport between carbon nanotubes in nanocomposites. *J Nanosci Nanotechnol* 2014;14(5):3696–702.
- [41] Sanati M, Sandwell A, Mostaghimi H, Park SS. Development of Nanocomposite-Based Strain Sensor with Piezoelectric and Piezoresistive Properties. *Sensors (Basel, Switzerland)* 2018, 18(11).
- [42] Paulson S, Falvo MR, Snider N, Helser A, Hudson T, Seeger A, et al. In situ resistance measurements of strained carbon nanotubes. *Appl Phys Lett* 1999;75(19):2936–8.
- [43] Panozzo F, Zappalorto M, Quaresimin M. Analytical model for the prediction of the piezoresistive behavior of CNT modified polymers. *Compos B Eng* 2017;109:53–63.
- [44] Hu B, Hu N, Li Y, Akagi K, Yuan W, Watanabe T, et al. Multi-scale numerical simulations on piezoresistivity of CNT/polymer nanocomposites. *Nanoscale Res Lett* 2012;7(1):1–11.
- [45] Gong J, Yang H, Yang P. Investigation on field emission properties of N-doped graphene-carbon nanotube composites. *Compos B Eng* 2015;75:250–5.
- [46] Hu N, Karube Y, Yan C, Masuda Z, Fukunaga H. Tunneling effect in a polymer/carbon nanotube nanocomposite strain sensor. *Acta Mater* 2008;56(13):2929–36.
- [47] Wu Di, Wei M, Li R, Xiao T, Gong S, Xiao Z, et al. A percolation network model to predict the electrical property of flexible CNT/PDMS composite films fabricated by spin coating technique. *Compos B Eng* 2019;174:107034. <https://doi.org/10.1016/j.compositesb.2019.107034>.
- [48] Liu Hu, Dong M, Huang W, Gao J, Dai K, Guo J, et al. Lightweight conductive graphene/thermoplastic polyurethane foams with ultrahigh compressibility for piezoresistive sensing. *J Mater Chem C* 2017;5(1):73–83.
- [49] Al-Saleh MH. Electrical and mechanical properties of graphene/carbon nanotube hybrid nanocomposites. *Synth Met* 2015;209:41–6.
- [50] Gao C, Zhang S, Wang F, Wen B, Han C, Ding Y, et al. Graphene networks with low percolation threshold in ABS nanocomposites: selective localization and electrical and rheological properties. *ACS Appl Mater Interfaces* 2014;6(15):12252–60.
- [51] Stankovich S, Dikin DA, Dommett GHB, Kohlhaas KM, Zimney EJ, Stach EA, et al. Nguyen ST, Ruoff RS. *Graphene-based composite materials*. *nature* 2006;442(7100):282–6.
- [52] Qi X-Y, Yan D, Jiang Z, Cao Y-K, Yu Z-Z, Yavari F, et al. Enhanced electrical conductivity in polystyrene nanocomposites at ultra-low graphene content. *ACS Appl Mater Interfaces* 2011;3(8):3130–3.
- [53] Hu N, Masuda Z, Yan C, Yamamoto Go, Fukunaga H, Hashida T. The electrical properties of polymer nanocomposites with carbon nanotube fillers. *Nanotechnology* 2008;19(21):215701. <https://doi.org/10.1088/0957-4484/19/21/215701>.
- [54] Jeong C, Park Y-B. Exfoliated Graphite Nanoplatelet-Carbon Nanotube Hybrid Composites for Compression Sensing. *ACS Omega* 2020;5(6):2630–9.
- [55] Tanabi H, Erdal M. Effect of CNTs dispersion on electrical, mechanical and strain sensing properties of CNT/epoxy nanocomposites. *Results Phys* 2019;12:486–503.
- [56] Tamburano A, Sarasini F, De Bellis G, D'Aloia AG, Sarto MS. The piezoresistive effect in graphene-based polymeric composites. *Nanotechnology* 2013;24(46):465702. <https://doi.org/10.1088/0957-4484/24/46/465702>.
- [57] Liebscher M, Domurath J, Saphiannikova M, Müller MT, Heinrich G, Pötschke P. Dispersion of graphite nanoplates in melt mixed PC/SAN polymer blends and its influence on rheological and electrical properties. *Polymer* 2020;200:122577. <https://doi.org/10.1016/j.polymer.2020.122577>.
- [58] Matos MAS, Tagarielli VL, Baiz-Villafranca PM, Pinho ST. Predictions of the electro-mechanical response of conductive CNT-polymer composites. *J Mech Phys Solids* 2018;114:84–96.
- [59] Hu N, Karube Y, Arai M, Watanabe T, Yan C, Li Y, et al. Investigation on sensitivity of a polymer/carbon nanotube composite strain sensor. *Carbon* 2010;48(3):680–7.